

Subcritical Hopf bifurcations in a car-following model with reaction-time delay

BY GÁBOR OROSZ^{1,*} AND GÁBOR STÉPÁN^{2,†}

¹*Bristol Centre for Applied Nonlinear Mathematics, Department of Engineering Mathematics, University of Bristol, Queen's Building, University Walk, Bristol BS8 1TR, UK*

²*Department of Applied Mechanics, Budapest University of Technology and Economics, PO Box 91, Budapest 1521, Hungary*

A nonlinear car-following model of highway traffic is considered, which includes the reaction-time delay of drivers. Linear stability analysis shows that the uniform flow equilibrium of the system loses its stability via Hopf bifurcations and thus oscillations can appear. The stability and amplitudes of the oscillations are determined with the help of normal-form calculations of the Hopf bifurcation that also handles the essential translational symmetry of the system. We show that the subcritical case of the Hopf bifurcation occurs robustly, which indicates the possibility of bistability. We also show how these oscillations lead to spatial wave formation as can be observed in real-world traffic flows.

Keywords: vehicular traffic; reaction-time delay; translational symmetry; subcritical Hopf bifurcation; bistability; stop-and-go waves

1. Introduction

The so-called *uniform flow equilibrium* of vehicles following each other on a road is a kind of steady state, where equidistant vehicles travel with the same constant velocity. Ideally, this state is stable. Indeed, it is the goal of traffic management that drivers choose their traffic parameters to keep this state stable and also to reach their goal, that is, to travel with a speed close to their desired speed. Still, traffic jams often appear as congestion waves travelling opposite to the flow of vehicles (Kerner 1999). The formation of these traffic jams (waves) is often associated with the linear instability of the uniform flow equilibrium, which should be a rare occurrence. However, it is also well known among traffic engineers that certain events, such as a truck pulling out of its lane, may trigger traffic jams even when the uniform flow is stable. We investigate a delayed car-following model and provide a thorough examination of the subcriticality of Hopf

* Author and address for correspondence: Applied Mathematics Group, Mathematics Research Institute, University of Exeter, Laver Building, North Park Road, Exeter EX4 4QE, UK (g.orosz@bristol.ac.uk).

† Alternative address: Research Group on Dynamics of Vehicles and Machines, Hungarian Academy of Science, PO Box 91, Budapest 1521, Hungary.

bifurcations related to the drivers' reaction-time delay. This explains how a stable uniform flow can coexist with a stable traffic wave.

The car-following model analysed in this paper was first introduced in Bando *et al.* (1995) without the reaction-time delay of drivers, and that was investigated by numerical simulation. Then, numerical continuation techniques were used in Gasser *et al.* (2004) and Berg & Wilson (2005) by applying the package AUTO (Doedel *et al.* 1997). Recently, Hopf calculations have been carried out in Gasser *et al.* (2004) for arbitrary numbers of cars following each other on a ring.

The reaction-time delay of drivers was first introduced in Bando *et al.* (1998), and its importance was then emphasized by the study of Davis (2003). In these papers, numerical simulation was used to explore the nonlinear dynamics of the system. The first systematic global bifurcation analysis of the delayed model (Davis 2003) was presented in Orosz *et al.* (2004), where numerical continuation techniques, namely the package DDE-BIFTOOL (Engelborghs *et al.* 2001), were used. The continuation results were extended to large numbers of cars in Orosz *et al.* (2005), where the dynamics of oscillations, belonging to different traffic patterns, were analysed as well. In this paper, we perform an analytical Hopf bifurcation calculation and determine the criticality of the bifurcation as a function of parameters for arbitrary numbers of vehicles in the presence of the drivers' reaction delay.

While the models without delay are described by ordinary differential equations (ODEs), presenting the dynamics in finite-dimensional phase spaces, the appearance of the delay leads to delay differential equations (DDEs) and to infinite-dimensional phase spaces. The finite-dimensional bifurcation theory that is available in basic textbooks (Guckenheimer & Holmes 1997; Kuznetsov 1998) have been extended to DDEs in Hale & Verduyn Lunel (1993), Diekmann *et al.* (1995), Kolmanovskii & Myshkis (1999) and Hale *et al.* (2002). The infinite-dimensional dynamics make the bifurcation analysis more abstract. In particular, the Hopf normal form calculations require complicated algebraic formalism and algorithms, as is shown in Hassard *et al.* (1981), Stépán (1986, 1989), Campbell & Bélair (1995), Orosz (2004) and Stone & Campbell (2004). Recently, these Hopf calculations have been extended for systems with translational symmetry in Orosz & Stépán (2004), which is an essential property of car-following models. This situation is similar to the S^1 symmetry that occurs in laser systems with delay, see Verduyn Lunel & Krauskopf (2000) and Rottschäfer & Krauskopf (2004). In Orosz & Stépán (2004), the method was demonstrated in the oversimplified case of two cars on a ring. Here, these calculations are extended to arbitrarily many cars, providing general conclusions for the subcriticality of the bifurcations and its consequences for flow patterns. Our results are generalization of those in Gasser *et al.* (2004) for the case without reaction-time delay. In particular, we prove that this delay makes the subcriticality of Hopf bifurcations robust.

2. Modelling issues

The mathematical form of the car-following model in question was introduced and non-dimensionalized in Orosz *et al.* (2004). Here, we recall the basic features of this model. Periodic boundary conditions are considered, i.e. n vehicles are

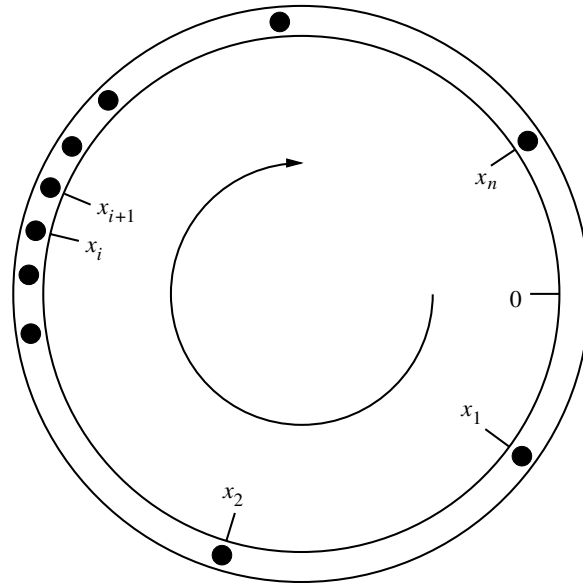


Figure 1. Vehicles flowing clockwise on a circular road.

distributed along a circular road of overall length L ; see figure 1. (This could be interpreted as traffic on a circular road around a large city, e.g. the M25 around London, even though such roads usually possess higher complexity.) As the number of cars is increased, the significance of the periodic boundary conditions usually tends to become smaller.

We assume that drivers have identical characteristics. Considering that the i th vehicle follows the $(i+1)$ th vehicle and the n th car follows the 1st one, the equations of motion can be expressed as

$$\left. \begin{aligned} \ddot{x}_i(t) &= \alpha(\mathbf{V}(x_{i+1}(t-1) - x_i(t-1)) - \dot{x}_i(t)), \quad i = 1, \dots, n-1, \\ \ddot{x}_n(t) &= \alpha(\mathbf{V}(x_1(t-1) - x_n(t-1) + L) - \dot{x}_n(t)), \end{aligned} \right\} \quad (2.1)$$

where the dot stands for time derivative. The position, the velocity, and the acceleration of the i th car are denoted by x_i , \dot{x}_i and \ddot{x}_i , respectively. The so-called *optimal velocity function* $\mathbf{V} : \mathbb{R}^+ \rightarrow \mathbb{R}^+$ depends on the distance of the cars $h_i = x_{i+1} - x_i$, which is usually called the *headway*. The argument of the headway contains the *reaction-time delay* of drivers which now is rescaled to 1. The parameter $\alpha > 0$ is known as the *sensitivity* and $1/\alpha > 0$ is often called the *relaxation time*. Due to the rescaling of the time with respect to the delay, the delay parameter is hidden in the sensitivity α and the magnitude of the function $\mathbf{V}(h)$; see details in Orosz *et al.* (2004).

Equation (2.1) expresses that each driver approaches an optimal velocity, given by $\mathbf{V}(h)$, with a characteristic relaxation time of $1/\alpha$, but reacts to its headway via a reaction-time delay 1. The general features of the optimal velocity function $\mathbf{V}(h)$ can be summarized as follows:

- (i) $\mathbf{V}(h)$ is continuous, non-negative and monotone increasing, since drivers want to travel faster as their headway increases. Note that in the vicinity

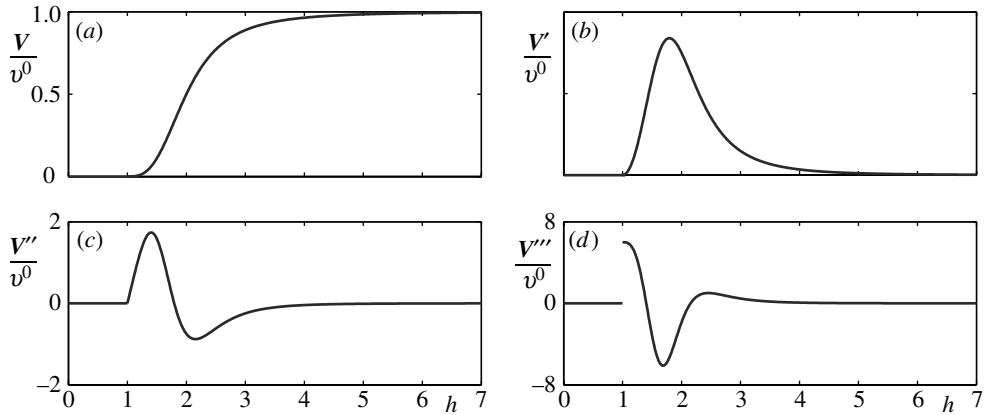


Figure 2. (a) The optimal velocity function (2.2) and (b–d) its derivatives.

of the Hopf bifurcation points, $\mathbf{V}(h)$ is required to be three times differentiable for the application of the Hopf theorem (Guckenheimer & Holmes 1997; Kuznetsov 1998).

- (ii) $\mathbf{V}(h) \rightarrow v^0$ as $h \rightarrow \infty$, where $v^0 > 0$ is known as the *desired speed*, which corresponds, for example, to the speed limit of the given highway. Drivers approach this speed with the relaxation time of $1/\alpha$ when the traffic is sparse.
- (iii) $\mathbf{V}(h) \equiv 0$ for $h \in [0, 1]$, where the so-called *jam headway* is rescaled to 1, see Orosz *et al.* (2004). This means that drivers attempt to come to a full stop if their headways become less than the jam headway.

One might, for example, consider the optimal velocity function to take the form

$$\mathbf{V}(h) = \begin{cases} 0, & \text{if } 0 \leq h \leq 1, \\ v^0 \frac{(h-1)^3}{1 + (h-1)^3}, & \text{if } h > 1, \end{cases} \quad (2.2)$$

as already used in Orosz *et al.* (2004, 2005). This function is shown together with its derivatives in figure 2. Functions with shapes similar to equation (2.2) were used in Bando *et al.* (1995, 1998) and Davis (2003).

Note that the analytical calculations presented here are valid for *any* optimal velocity function $\mathbf{V}(h)$: it is not necessary to restrict oneself to a concrete function in contrast to the numerical simulations in Bando *et al.* (1998) and Davis (2003) and even to the numerical continuations in Orosz *et al.* (2004, 2005).

The dimensionless parameters α and v^0 can be obtained from their dimensional counterparts as shown in Orosz *et al.* (2004). If we consider the reaction-time delay 1–2 s and the relaxation time 1–50 s, we obtain the sensitivity as their ratio: $\alpha \in [0.02, 2]$. Also, if we assume desired speeds in the range 10–40 m s⁻¹ and jam headways 5–10 m, their ratio times the reaction time provides the dimensionless desired speed $v^0 \in [1, 20]$. The linear stability diagram does not change qualitatively when v^0 is varied in this range as shown in Orosz *et al.* (2005).

3. Translational symmetry and Hopf bifurcations

The stationary motion of the vehicles, the so-called *uniform flow equilibrium*, is described by

$$x_i^{\text{eq}}(t) = v^*t + x_i^*, \quad \Rightarrow \quad \dot{x}_i^{\text{eq}}(t) \equiv v^*, \quad i = 1, \dots, n, \quad (3.1)$$

where

$$x_{i+1}^* - x_i^* = x_1^* - x_n^* + L = L/n := h^*, \quad i = 1, \dots, n-1, \quad (3.2)$$

and

$$v^* = \mathbf{V}(h^*) < v^0. \quad (3.3)$$

Note that one of the constants x_i^* can be chosen arbitrarily due to the translational symmetry along the ring. Henceforward, we consider the *average headway* $h^* = L/n$ as a bifurcation parameter. Increasing h^* increases the length L of the ring, which involves scaling all headways h_i accordingly.

Let us define the perturbation of the uniform flow equilibrium by

$$x_i^{\text{p}}(t) := x_i(t) - x_i^{\text{eq}}(t), \quad i = 1, \dots, n. \quad (3.4)$$

Using Taylor series expansion of the optimal velocity function $\mathbf{V}(h)$ about $h = h^* (=L/n)$ up to third order of x_i^{p} , we can eliminate the zero-order terms

$$\left. \begin{aligned} \ddot{x}_i^{\text{p}}(t) &= -\alpha \dot{x}_i^{\text{p}}(t) + \alpha \sum_{k=1}^3 b_k(h^*) (x_{i+1}^{\text{p}}(t-1) - x_i^{\text{p}}(t-1))^k, \quad i = 1, \dots, n-1, \\ \ddot{x}_n^{\text{p}}(t) &= -\alpha \dot{x}_n^{\text{p}}(t) + \alpha \sum_{k=1}^3 b_k(h^*) (x_1^{\text{p}}(t-1) - x_n^{\text{p}}(t-1))^k, \end{aligned} \right\} \quad (3.5)$$

where

$$b_1(h^*) = \mathbf{V}'(h^*), \quad b_2(h^*) = \frac{1}{2} \mathbf{V}''(h^*), \quad \text{and} \quad b_3(h^*) = \frac{1}{6} \mathbf{V}'''(h^*). \quad (3.6)$$

At a critical/bifurcation point h_{cr}^* , the derivatives take the values $b_{1\text{cr}} = \mathbf{V}'(h_{\text{cr}}^*)$, $b_{2\text{cr}} = (1/2) \mathbf{V}''(h_{\text{cr}}^*)$ and $b_{3\text{cr}} = (1/6) \mathbf{V}'''(h_{\text{cr}}^*)$. Now, and further on, prime denotes differentiation with respect to the headway.

Introducing the notation

$$y_i(t) := \dot{x}_i^{\text{p}}(t), \quad y_{i+n}(t) := x_i^{\text{p}}(t), \quad i = 1, \dots, n, \quad (3.7)$$

equation (3.5) can be rewritten as

$$\dot{y}(t) = \tilde{\mathbf{L}}(h^*)y(t) + \tilde{\mathbf{R}}(h^*)y(t-1) + \tilde{F}(y(t-1); h^*), \quad (3.8)$$

where $y: \mathbb{R} \rightarrow \mathbb{R}^{2n}$. The matrices $\tilde{\mathbf{L}}, \tilde{\mathbf{R}}: \mathbb{R} \rightarrow \mathbb{R}^{2n \times 2n}$ and the near-zero analytic function $\tilde{F}: \mathbb{R}^{2n} \times \mathbb{R} \rightarrow \mathbb{R}^{2n}$ are defined as

$$\begin{aligned} \tilde{\mathbf{L}}(h^*) &\equiv \begin{bmatrix} -\alpha \mathbf{I} & 0 \\ \mathbf{I} & 0 \end{bmatrix}, \quad \tilde{\mathbf{R}}(h^*) = \begin{bmatrix} 0 & -\alpha b_1(h^*)A \\ 0 & 0 \end{bmatrix}, \quad \text{and} \\ \tilde{F}(y(t-1); h^*) &= \begin{bmatrix} \alpha b_2(h^*)F_2(y(t-1)) + \alpha b_3(h^*)F_3(y(t-1)) \\ 0 \end{bmatrix}. \end{aligned} \quad (3.9)$$

Here, $I \in \mathbb{R}^{n \times n}$ stands for the n -dimensional identity matrix, while the matrix $A \in \mathbb{R}^{n \times n}$ and the functions $F_2, F_3 : \mathbb{R}^{2n} \rightarrow \mathbb{R}^n$ are defined as

$$A = \begin{bmatrix} \ddots & \ddots & & & & \\ & & 1 & -1 & & \\ & & & \ddots & \ddots & \\ -1 & & & & & \ddots \end{bmatrix}, \quad F_k(y(t-1)) = \begin{bmatrix} (y_{n+2}(t-1) - y_{n+1}(t-1))^k \\ (y_{n+3}(t-1) - y_{n+2}(t-1))^k \\ \vdots \\ (y_{n+1}(t-1) - y_{2n}(t-1))^k \end{bmatrix}, \quad k = 2, 3. \tag{3.10}$$

System (3.8) possesses a translational symmetry, therefore, the matrices $\tilde{L}(h^*), \tilde{R}(h^*)$ satisfy

$$\det(\tilde{L}(h^*) + \tilde{R}(h^*)) = 0, \tag{3.11}$$

that is, the Jacobian $(\tilde{L}(h^*) + \tilde{R}(h^*))$ has a zero eigenvalue

$$\lambda_0(h^*) = 0, \tag{3.12}$$

for any value of parameter h^* . Furthermore, the near-zero analytic function \tilde{F} preserves this translational symmetry, that is,

$$\tilde{F}(y(t-1) + c; h^*) = \tilde{F}(y(t-1); h^*), \tag{3.13}$$

for all $c \neq 0$ satisfying $(\tilde{L}(h^*) + \tilde{R}(h^*))c = 0$; see details in [Orosz & Stépán \(2004\)](#).

The steady state $y(t) \equiv 0$ of equation (3.8) corresponds to the uniform flow equilibrium (3.1) of the original system (2.1). Considering the linear part of (3.8) and using the trial solution $y(t) = Ce^{\lambda t}$ with $C \in \mathbb{C}^{2n}$ and $\lambda \in \mathbb{C}$, the characteristic equation becomes

$$D(\lambda; b_1(h^*)) = (\lambda^2 + \alpha\lambda + \alpha b_1(h^*)e^{-\lambda})^n - (\alpha b_1(h^*)e^{-\lambda})^n = 0. \tag{3.14}$$

According to equation (3.11), the relevant zero eigenvalue (3.12) is one of the infinitely many characteristic exponents that satisfy equation (3.14). This exponent exists for any value of the parameter b_1 , that is, for any value of the bifurcation parameter h^* .

At a bifurcation point defined by $b_1 = b_{1cr}$, i.e. by $h^* = h_{cr}^*$, Hopf bifurcations may occur in the complementary part of the phase space spanned by the eigenspace of the zero exponent (3.12). Then, there exists a complex conjugate pair of pure imaginary characteristic exponents

$$\lambda_{1,2}(h_{cr}^*) = \pm i\omega, \quad \omega \in \mathbb{R}^+, \tag{3.15}$$

which satisfies equation (3.14). To find the Hopf boundaries in the parameter space, we substitute $\lambda_1 = i\omega$ into equation (3.14). Separation of the real and imaginary parts gives

$$\left. \begin{aligned} b_{1cr} &= \frac{\omega}{2 \cos\left(\omega - \frac{k\pi}{n}\right) \sin\left(\frac{k\pi}{n}\right)}, \\ \alpha &= -\omega \cot\left(\omega - \frac{k\pi}{n}\right). \end{aligned} \right\} \tag{3.16}$$

The so-called wave number k can take the values $k = 1, \dots, n/2$ (for even n) and $k = 1, \dots, (n-1)/2$ (for odd n). The wave numbers $k > n/2$ are not considered since they belong to conjugated waves producing the same spatial pattern. Note that $k=1$ belongs to the stability boundary of the uniform flow equilibrium, while the cases $k > 1$ result in further oscillation modes around the already unstable equilibrium. Furthermore, for each k the resulting frequency is bounded so that $\omega \in (0, k\pi/n)$; see Orosz *et al.* (2004, 2005).

Note also that the function $b_1(h^*) = \mathbf{V}'(h^*)$ shown in figure 2*b* is non-monotonous, and so a b_{1cr} boundary typically leads either to two or to zero h_{cr}^* boundaries. For a fixed wave number k , these boundaries tend to finite values of h^* as $n \rightarrow \infty$, as is shown in Orosz *et al.* (2005). Using trigonometric identities, equation (3.16) can be transformed to

$$\left. \begin{aligned} \cos \omega &= \frac{\omega}{2b_{1cr}} \left(\frac{\omega}{\alpha} + \cot \left(\frac{k\pi}{n} \right) \right), \\ \sin \omega &= \frac{\omega}{2b_{1cr}} \left(1 - \frac{\omega}{\alpha} \cot \left(\frac{k\pi}{n} \right) \right), \end{aligned} \right\} \quad (3.17)$$

which is a useful form used later in the Hopf calculation together with the resulting form

$$\frac{4b_{1cr}^2}{\omega^2} \sin^2 \left(\frac{k\pi}{n} \right) = 1 + \frac{\omega^2}{\alpha^2}. \quad (3.18)$$

With the help of the identity

$$\frac{(1 + i \cot(\frac{k\pi}{n}))^{n-1}}{(1 - i \cot(\frac{k\pi}{n}))^{n-1}} = \frac{1 - i \cot(\frac{k\pi}{n})}{1 + i \cot(\frac{k\pi}{n})}, \quad (3.19)$$

we can calculate the following necessary condition for Hopf bifurcation as the parameter b_1 is varied as

$$\operatorname{Re} \left(\frac{d\lambda_1(b_{1cr})}{db_1} \right) = \operatorname{Re} \left(- \frac{\partial D(\lambda_1; b_{1cr})}{\partial b_1} \left(\frac{\partial D(\lambda_1; b_{1cr})}{\partial \lambda} \right)^{-1} \right) = \mathcal{E} \frac{1}{b_{1cr}} (\omega^2 + \alpha^2 + \alpha) > 0, \quad (3.20)$$

where

$$\mathcal{E} = \left(\left(\frac{\alpha}{\omega} - \omega \right)^2 + (2 + \alpha)^2 \right)^{-1}. \quad (3.21)$$

Since equation (3.20) is always positive, this Hopf condition is always satisfied. Now, using the chain rule and definition (3.6), condition (3.20) can be calculated further as the average headway h^* is varied to give

$$\operatorname{Re}(\lambda_1'(h_{cr}^*)) = \operatorname{Re} \left(\frac{d\lambda_1(b_{1cr})}{db_1} b_1'(h_{cr}^*) \right) = \mathcal{E} \frac{2b_{2cr}}{b_{1cr}} (\omega^2 + \alpha^2 + \alpha) \neq 0. \quad (3.22)$$

This condition is fulfilled if and only if $b_{2cr} \neq 0$, which is usually satisfied except at some special points. For example, the function $\mathbf{V}''(h)$ shown in figure 2*c* becomes zero at a single point over the interval $h \in (1, \infty)$. Notice that $\mathbf{V}''(h)$ is zero for

$h \in [0, 1]$ and for $h \rightarrow \infty$, but the critical headway h_{cr} never takes these values for $\alpha > 0$. Conditions (3.20) and (3.22) ensure that the characteristic roots (3.15) cross the imaginary axis with a non-zero speed when the parameters b_1 and h^* are varied.

4. Operator differential equations and related eigenvectors

The DDE (3.8) can be rewritten in the form of an operator differential equation (OpDE) which reflects its infinite-dimensional dynamics. For the critical bifurcation parameter h_{cr}^* , we obtain

$$\dot{y}_t = \mathcal{A}y_t + \mathcal{F}(y_t), \tag{4.1}$$

where the dot still refers to differentiation with respect to the time t and $y_t : \mathbb{R} \rightarrow \mathbb{X}_{\mathbb{R}^{2n}}$ is defined by the shift $y_t(\vartheta) = y(t + \vartheta)$, $\vartheta \in [-1, 0]$ on the function space $\mathbb{X}_{\mathbb{R}^{2n}}$ of continuous functions mapping $[-1, 0] \rightarrow \mathbb{R}^{2n}$. The linear and nonlinear operators $\mathcal{A}, \mathcal{F} : \mathbb{X}_{\mathbb{R}^{2n}} \rightarrow \mathbb{X}_{\mathbb{R}^{2n}}$ are defined as

$$\mathcal{A}\phi(\vartheta) = \begin{cases} \frac{\partial}{\partial \vartheta} \phi(\vartheta), & \text{if } -1 \leq \vartheta < 0, \\ \mathbf{L}\phi(0) + \mathbf{R}\phi(-1), & \text{if } \vartheta = 0, \end{cases} \tag{4.2}$$

$$\mathcal{F}(\phi)(\vartheta) = \begin{cases} 0, & \text{if } -1 \leq \vartheta < 0, \\ F(\phi(-1)), & \text{if } \vartheta = 0, \end{cases} \tag{4.3}$$

where the matrices $\mathbf{L}, \mathbf{R} \in \mathbb{R}^{2n \times 2n}$ and the nonlinear function $F : \mathbb{R}^{2n} \rightarrow \mathbb{R}^{2n}$ are given by

$$\mathbf{L} = \tilde{\mathbf{L}}(h_{cr}^*), \quad \mathbf{R} = \tilde{\mathbf{R}}(h_{cr}^*), \quad \text{and} \quad F(y(t-1)) = \tilde{F}(y(t-1); h_{cr}^*). \tag{4.4}$$

The translational symmetry conditions (3.11) and (3.13) are inherited, that is,

$$\det(\mathbf{L} + \mathbf{R}) = 0, \tag{4.5}$$

and

$$\mathcal{F}(y_t + c) = \mathcal{F}(y_t) \Leftrightarrow F(y(t-1) + c) = F(y(t-1)), \tag{4.6}$$

for all $c \neq 0$ satisfying $(\mathbf{L} + \mathbf{R})c = 0$.

In order to avoid singularities in Hopf calculations, we follow the methodology and algorithm of [Orosz & Stépán \(2004\)](#) and eliminate the eigendirection belonging to the relevant zero eigenvalue $\lambda_0 = 0$ (equation (3.12)). The corresponding eigenvector $s_0 \in \mathbb{X}_{\mathbb{R}^{2n}}$ satisfies

$$\mathcal{A}s_0 = \lambda_0 s_0 \Rightarrow \mathcal{A}s_0 = 0, \tag{4.7}$$

which, applying the definition (4.2) of operator \mathcal{A} , leads to a boundary value problem with the constant solution

$$s_0(\vartheta) \equiv S_0 \in \mathbb{R}^{2n}, \quad \text{satisfying } (\mathbf{L} + \mathbf{R})S_0 = 0. \tag{4.8}$$

One finds that

$$S_0 = p \begin{bmatrix} 0 \\ E \end{bmatrix}, \tag{4.9}$$

where each component of the vector $E \in \mathbb{R}^n$ is equal to 1. Here, $p \in \mathbb{R}$ is a scalar that can be chosen freely, in particular, we choose

$$p = 1. \quad (4.10)$$

In order to project the system to s_0 and to its complementary space, we also need the adjoint operator

$$\mathcal{A}^* \psi(\sigma) = \begin{cases} -\frac{\partial}{\partial \sigma} \psi(\sigma), & \text{if } 0 \leq \sigma < 1, \\ \mathbf{L}^* \psi(0) + \mathbf{R}^* \psi(1), & \text{if } \sigma = 0, \end{cases} \quad (4.11)$$

where asterisk denotes either adjoint operator or transposed conjugate vector and matrix. The eigenvector $n_0 \in \mathbb{X}_{\mathbb{R}^{2n}}^*$ of \mathcal{A}^* associated with the eigenvalue $\lambda_0^* = 0$ satisfies

$$\mathcal{A}^* n_0 = \lambda_0^* n_0 \Rightarrow \mathcal{A}^* n_0 = 0. \quad (4.12)$$

This gives another boundary value problem, which has the constant solution

$$n_0(\sigma) \equiv N_0 \in \mathbb{R}^{2n}, \quad \text{satisfying } (\mathbf{L}^* + \mathbf{R}^*) N_0 = 0. \quad (4.13)$$

Here, we obtain

$$N_0 = \hat{p} \begin{bmatrix} E \\ \alpha E \end{bmatrix}. \quad (4.14)$$

However, $\hat{p} \in \mathbb{R}$ is not free, but is determined by the normality condition

$$\langle n_0, s_0 \rangle = 1. \quad (4.15)$$

Defining the inner product

$$\langle \psi, \phi \rangle = \psi^*(0) \phi(0) + \int_{-1}^0 \psi^*(\xi + 1) \mathbf{R} \phi(\xi) d\xi, \quad (4.16)$$

condition (4.15) gives the scalar equation

$$N_0^* (\mathbf{I} + \mathbf{R}) S_0 = 1, \quad (4.17)$$

from which we obtain

$$\hat{p} = \frac{1}{n\alpha}. \quad (4.18)$$

Note that, as the vectors s_0 and n_0 are the right and left eigenvectors of the operator \mathcal{A} belonging to the eigenvalues $\lambda_0 = 0$ and $\lambda_0^* = 0$, similarly, the vectors S_0 and N_0 are the right and left eigenvectors of the matrix $(\mathbf{L} + \mathbf{R}e^{-\lambda})$, belonging to the same zero eigenvalues. For the non-delayed model (Bando *et al.* 1995), the vectors S_0 and N_0 are the left and right eigenvectors of the Jacobian $(\mathbf{L} + \mathbf{R})$, that is, their structure is related the spatial structure of the system along the circular road.

We are now able to eliminate the singular dynamics generated by the translational symmetry so that we project the system to s_0 and to its complementary space. With the help of the eigenvectors s_0 and n_0 , the new state variables $z_0 : \mathbb{R} \rightarrow \mathbb{R}$ and $y_t^- : \mathbb{R} \rightarrow \mathbb{X}_{\mathbb{R}^{2n}}$ are defined as

$$\begin{cases} z_0 = \langle n_0, y_t \rangle, \\ y_t^- = y_t - z_0 s_0. \end{cases} \quad (4.19)$$

Using the derivation given in Orosz & Stépán (2004), we split the OpDE (4.1) into

$$\left. \begin{aligned} \dot{z}_0 &= N_0^* \mathcal{F}(y_t^-)(0), \\ \dot{y}_t^- &= \mathcal{A}y_t^- + \mathcal{F}(y_t^-) - N_0^* \mathcal{F}(y_t^-)(0)S_0. \end{aligned} \right\} \tag{4.20}$$

Its second part is already fully decoupled, and can be redefined as

$$\dot{y}_t^- = \mathcal{A}y_t^- + \mathcal{F}^-(y_t^-), \tag{4.21}$$

where the new nonlinear operator $\mathcal{F}^- : \mathbb{X}_{\mathbb{R}^{2n}} \rightarrow \mathbb{X}_{\mathbb{R}^{2n}}$ assumes the form

$$\mathcal{F}^-(\phi)(\vartheta) = \begin{cases} -N_0^* \mathcal{F}(\phi)(0)S_0, & \text{if } -1 \leq \vartheta < 0, \\ \mathcal{F}(\phi)(0) - N_0^* \mathcal{F}(\phi)(0)S_0, & \text{if } \vartheta = 0. \end{cases} \tag{4.22}$$

Considering $\mathcal{F}(\phi)(0) = F(\phi(-1))$ given by equation (4.3), and using the expressions (3.9), (3.10) and (4.4), and the eigenvectors (4.9) and (4.14), we obtain

$$\begin{aligned} N_0^* \mathcal{F}(y_t^-)(0)S_0 &= N_0^* F(y(t-1))S_0 \\ &= \frac{1}{n} \sum_{k=2,3} \left(b_{\text{kr}} \sum_{i=1}^n (y_{n+i+1}(t-1) - y_{n+i}(t-1))^k \right) \begin{bmatrix} 0 \\ E \end{bmatrix}, \end{aligned} \tag{4.23}$$

where the definition $y_{2n+1} := y_{n+1}$ is applied. Note that the system reduction related to the translational symmetry changes the nonlinear operator of the system while the linear operator remains the same. This change has an essential role in the centre-manifold reduction presented below.

Let us consider a Hopf bifurcation at a critical point h_{cr}^* . First, we determine the real and imaginary parts $s_1, s_2 \in \mathbb{X}_{\mathbb{R}^{2n}}$ of the eigenvector of the linear operator \mathcal{A} , which belongs to the critical eigenvalue $\lambda_1 = i\omega$ (3.15), that is,

$$\mathcal{A}(s_1 + is_2) = \lambda_1(s_1 + is_2) \Rightarrow \mathcal{A}s_1 = -\omega s_2, \quad \mathcal{A}s_2 = \omega s_1. \tag{4.24}$$

After the substitution of definition (4.2) of \mathcal{A} , the solution of the resulting boundary value problem can be written as

$$\begin{bmatrix} s_1(\vartheta) \\ s_2(\vartheta) \end{bmatrix} = \begin{bmatrix} S_1 \\ S_2 \end{bmatrix} \cos(\omega\vartheta) + \begin{bmatrix} -S_2 \\ S_1 \end{bmatrix} \sin(\omega\vartheta), \tag{4.25}$$

with constant vectors $S_1, S_2 \in \mathbb{R}^{2n}$ satisfying the homogeneous equation

$$\begin{bmatrix} \mathbf{L} + \mathbf{R} \cos \omega & \omega \mathbf{I} + \mathbf{R} \sin \omega \\ -(\omega \mathbf{I} + \mathbf{R} \sin \omega) & \mathbf{L} + \mathbf{R} \cos \omega \end{bmatrix} \begin{bmatrix} S_1 \\ S_2 \end{bmatrix} = \begin{bmatrix} 0 \\ 0 \end{bmatrix}. \tag{4.26}$$

Using formula (3.17) and following the steps (A 1)–(A 3) of appendix A, one may solve (4.26) and obtain

$$S_1 = u \begin{bmatrix} C \\ \frac{1}{\omega} S \end{bmatrix} + v \begin{bmatrix} S \\ -\frac{1}{\omega} C \end{bmatrix}, \quad S_2 = u \begin{bmatrix} S \\ -\frac{1}{\omega} C \end{bmatrix} - v \begin{bmatrix} C \\ \frac{1}{\omega} S \end{bmatrix}, \tag{4.27}$$

where the scalar parameters u and v can be chosen arbitrarily and the vectors C , $S \in \mathbb{R}^n$ are

$$C = \begin{bmatrix} \cos\left(\frac{2k\pi}{n} 1\right) \\ \cos\left(\frac{2k\pi}{n} 2\right) \\ \vdots \\ \cos\left(\frac{2k\pi}{n} n\right) \end{bmatrix}, \quad S = \begin{bmatrix} \sin\left(\frac{2k\pi}{n} 1\right) \\ \sin\left(\frac{2k\pi}{n} 2\right) \\ \vdots \\ \sin\left(\frac{2k\pi}{n} n\right) \end{bmatrix}, \quad (4.28)$$

with the wave number k used in equations (3.16) and (3.17). The cyclic permutation of the components in C and S results in further vectors S_1 and S_2 that still satisfy equation (4.26). This result corresponds to the \mathbb{Z}^n symmetry of the system, that is, all the cars have the same dynamic characteristics. Choosing $u=1$ and $v=0$ yields

$$S_1 = \begin{bmatrix} C \\ \frac{1}{\omega} S \end{bmatrix}, \quad S_2 = \begin{bmatrix} S \\ -\frac{1}{\omega} C \end{bmatrix}. \quad (4.29)$$

The real and imaginary parts $n_1, n_2 \in \mathbb{X}_{\mathbb{R}^{2n}}^*$ of the eigenvector of the adjoint operator \mathcal{A}^* associated with $\lambda_1^* = -i\omega$ are determined by

$$\mathcal{A}^*(n_1 + in_2) = \lambda_1^*(n_1 + in_2) \Rightarrow \mathcal{A}^*n_1 = \omega n_2, \quad \mathcal{A}^*n_2 = -\omega n_1. \quad (4.30)$$

The use of definition (4.11) of \mathcal{A}^* leads to another boundary value problem having the solution

$$\begin{bmatrix} n_1(\sigma) \\ n_2(\sigma) \end{bmatrix} = \begin{bmatrix} N_1 \\ N_2 \end{bmatrix} \cos(\omega\sigma) + \begin{bmatrix} -N_2 \\ N_1 \end{bmatrix} \sin(\omega\sigma), \quad (4.31)$$

where the constant vectors $N_1, N_2 \in \mathbb{R}^{2n}$ satisfy

$$\begin{bmatrix} \mathbf{L}^* + \mathbf{R}^* \cos \omega & -(\omega \mathbf{I} + \mathbf{R}^* \sin \omega) \\ \omega \mathbf{I} + \mathbf{R}^* \sin \omega & \mathbf{L}^* + \mathbf{R}^* \cos \omega \end{bmatrix} \begin{bmatrix} N_1 \\ N_2 \end{bmatrix} = \begin{bmatrix} 0 \\ 0 \end{bmatrix}. \quad (4.32)$$

Applying equation (3.17) and following the steps (A 4)–(A 7) of appendix A, the solution of equation (4.32) is obtained as

$$\begin{aligned} N_1 &= \hat{u} \begin{bmatrix} C \\ \alpha C + \omega S \end{bmatrix} + \hat{v} \begin{bmatrix} S \\ \alpha S - \omega C \end{bmatrix}, \\ N_2 &= \hat{u} \begin{bmatrix} S \\ \alpha S - \omega C \end{bmatrix} - \hat{v} \begin{bmatrix} C \\ \alpha C + \omega S \end{bmatrix}. \end{aligned} \quad (4.33)$$

The scalar parameters \hat{u}, \hat{v} are determined by the orthonormality conditions

$$\langle n_1, s_1 \rangle = 1, \quad \langle n_1, s_2 \rangle = 0, \tag{4.34}$$

which using the inner product definition (4.16), results in the two scalar equations

$$\frac{1}{2} \begin{bmatrix} S_1^* \left(2I + R^* \left(\cos \omega + \frac{\sin \omega}{\omega} \right) \right) + S_2^* R^* \sin \omega & -S_1^* R^* \sin \omega + S_2^* R^* \left(\cos \omega - \frac{\sin \omega}{\omega} \right) \\ -S_1^* R^* \sin \omega + S_2^* \left(2I + R^* \left(\cos \omega + \frac{\sin \omega}{\omega} \right) \right) & -S_1^* R^* \left(\cos \omega - \frac{\sin \omega}{\omega} \right) - S_2^* R^* \sin \omega \end{bmatrix} \times \begin{bmatrix} N_1 \\ N_2 \end{bmatrix} = \begin{bmatrix} 1 \\ 0 \end{bmatrix}. \tag{4.35}$$

Substituting equations (3.17), (4.29) and (4.33) into (4.35) and using the second-order trigonometric identities (B 3)–(B 5) of appendix B, we obtain

$$\frac{n}{2} \begin{bmatrix} 2 + \alpha & \frac{\alpha}{\omega} - \omega \\ -\left(\frac{\alpha}{\omega} - \omega \right) & 2 + \alpha \end{bmatrix} \begin{bmatrix} \hat{u} \\ \hat{v} \end{bmatrix} = \begin{bmatrix} 1 \\ 0 \end{bmatrix}, \tag{4.36}$$

with the solution

$$\begin{bmatrix} \hat{u} \\ \hat{v} \end{bmatrix} = \mathcal{E} \frac{2}{n} \begin{bmatrix} 2 + \alpha \\ \frac{\alpha}{\omega} - \omega \end{bmatrix}, \tag{4.37}$$

where \mathcal{E} is defined by equation (3.21). The substitution of equation (4.37) into (4.33) leads to

$$N_1 = \mathcal{E} \frac{2}{n} \begin{bmatrix} (2 + \alpha)C + \left(\frac{\alpha}{\omega} - \omega \right)S \\ (\alpha^2 + \alpha + \omega^2)C + \left(\frac{\alpha^2}{\omega} + 2\omega \right)S \end{bmatrix}, \tag{4.38}$$

$$N_2 = \mathcal{E} \frac{2}{n} \begin{bmatrix} (2 + \alpha)S - \left(\frac{\alpha}{\omega} - \omega \right)C \\ (\alpha^2 + \alpha + \omega^2)S - \left(\frac{\alpha^2}{\omega} + 2\omega \right)C \end{bmatrix}.$$

As $s_1 + is_2$ and $n_1 + in_2$ are the right and left eigenvectors of the operator \mathcal{A} belonging to the eigenvalues $\lambda_1 = i\omega$ and $\lambda_1^* = -i\omega$, the vectors $S_1 + iS_2$ and $N_1 + iN_2$ are similarly the right and left eigenvectors of the matrix $(L + Re^{-\lambda})$

belonging to the same eigenvalues. Note that for the non-delayed model (Bando *et al.* 1995) the vectors $S_1 + iS_2$ and $N_1 + iN_2$ are the left and right eigenvectors of the Jacobian ($\mathbf{L} + \mathbf{R}$), that is, their structure is again related the spatial structure of the system.

5. Centre-manifold reduction

Now, we investigate the essential dynamics on the two-dimensional centre manifold embedded in the infinite-dimensional phase space. Since the eigenvectors s_1 and s_2 span a plane tangent to the centre manifold at the origin, we use s_1 , s_2 and n_1 , n_2 to introduce the new state variables

$$\begin{cases} z_1 = \langle n_1, y_t^- \rangle, \\ z_2 = \langle n_2, y_t^- \rangle, \\ w = y_t^- - z_1 s_1 - z_2 s_2, \end{cases} \quad (5.1)$$

where $z_1, z_2 : \mathbb{R} \rightarrow \mathbb{R}$ and $w : \mathbb{R} \rightarrow \mathbb{X}_{\mathbb{R}^{2n}}$. Using the derivation presented in Orosz & Stépán (2004), we can reduce OpDE (4.21) to the form

$$\begin{aligned} \begin{bmatrix} \dot{z}_1 \\ \dot{z}_2 \\ \dot{w} \end{bmatrix} &= \begin{bmatrix} 0 & \omega & \mathcal{O} \\ -\omega & 0 & \mathcal{O} \\ 0 & 0 & \mathcal{A} \end{bmatrix} \begin{bmatrix} z_1 \\ z_2 \\ w \end{bmatrix} \\ &+ \begin{bmatrix} (N_1^* - q_1 N_0^*) \mathcal{F}(z_1 s_1 + z_2 s_2 + w)(0) \\ (N_2^* - q_2 N_0^*) \mathcal{F}(z_1 s_1 + z_2 s_2 + w)(0) \\ -\sum_{j=1,2} (N_j^* - q_j N_0^*) \mathcal{F}(z_1 s_1 + z_2 s_2 + w)(0) s_j + \mathcal{F}^-(z_1 s_1 + z_2 s_2 + w) \end{bmatrix}. \end{aligned} \quad (5.2)$$

The scalar parameters q_1, q_2 are induced by the translational symmetry and their expressions are determined in Orosz & Stépán (2004) as

$$\left. \begin{aligned} q_1 &= \left(N_1^* \left(\mathbf{I} + \frac{\sin \omega}{\omega} \mathbf{R} \right) - N_2^* \frac{1 - \cos \omega}{\omega} \mathbf{R} \right) S_0, \\ q_2 &= \left(N_1^* \frac{1 - \cos \omega}{\omega} \mathbf{R} + N_2^* \left(\mathbf{I} + \frac{\sin \omega}{\omega} \mathbf{R} \right) \right) S_0. \end{aligned} \right\} \quad (5.3)$$

Since in our case $\mathbf{R}S_0 = N_1^* S_0 = N_2^* S_0 = 0$, we obtain

$$q_1 = q_2 = 0. \quad (5.4)$$

The power series form of (5.2) is also given in Orosz & Stépán (2004) as

$$\begin{aligned}
 \begin{bmatrix} \dot{z}_1 \\ \dot{z}_2 \\ \dot{w} \end{bmatrix} &= \begin{bmatrix} 0 & \omega & \mathcal{O} \\ -\omega & 0 & \mathcal{O} \\ 0 & 0 & \mathcal{A} \end{bmatrix} \begin{bmatrix} z_1 \\ z_2 \\ w \end{bmatrix} + \begin{bmatrix} \sum_{j,k \geq 0}^{j+k=2,3} f_{jk}^{(1)} z_1^j z_2^k \\ \sum_{j,k \geq 0}^{j+k=2,3} f_{jk}^{(2)} z_1^j z_2^k \\ \frac{1}{2} \sum_{j,k \geq 0}^{j+k=2} (F_{jk}^{(3c)} \cos(\omega\vartheta) + F_{jk}^{(3s)} \sin(\omega\vartheta)) z_1^j z_2^k \end{bmatrix} \\
 &+ \begin{bmatrix} F_{10}^{(1)*} \mathbf{R}w(-1)z_1 + F_{01}^{(1)*} \mathbf{R}w(-1)z_2 \\ F_{10}^{(2)*} \mathbf{R}w(-1)z_1 + F_{01}^{(2)*} \mathbf{R}w(-1)z_2 \\ \frac{1}{2} \begin{cases} \sum_{j,k \geq 0}^{j+k=2} F_{jk}^{(3-)} z_1^j z_2^k, & \text{if } -1 \leq \vartheta < 0, \\ \sum_{j,k \geq 0}^{j+k=2} (F_{jk}^{(3)} + F_{jk}^{(3-)}) z_1^j z_2^k, & \text{if } \vartheta = 0 \end{cases} \end{bmatrix}, \tag{5.5}
 \end{aligned}$$

where the subscripts of the constant coefficients $f_{jk}^{(i)} \in \mathbb{R}$ and the vector ones $F_{jk}^{(i)} \in \mathbb{R}^{2n}$ refer to the corresponding j th and k th orders of z_1 and z_2 , respectively. The terms with the coefficients $F_{jk}^{(3c)}$ and $F_{jk}^{(3s)}$ come from the linear combinations of $s_1(\vartheta)$ and $s_2(\vartheta)$. The translational symmetry only enters through the terms with coefficients $F_{jk}^{(3-)}$, so that the terms with coefficients $F_{jk}^{(3)}$ and $F_{jk}^{(3-)}$ refer to the structure of the modified nonlinear operator \mathcal{F}^- (equation (4.22)). Using the third- and fourth-order trigonometric identities (B 6)–(B 11) of appendix B, we can calculate these coefficients for wave numbers $k \neq n/2$, $k \neq n/3$ and $k \neq n/4$ as given by equations (A 8) and (A 9) in appendix A.

Note that the cases $k = n/2$, $k = n/3$ and $k = n/4$ result in different formulae for the above coefficients, but the final Poincaré–Lyapunov constant will have the same formula as in the case of general wave number k . The detailed calculation of these ‘resonant’ cases is not presented here.

Approximate the centre manifold locally as a truncated power series of w depending on the coordinates z_1 and z_2 as

$$w(\vartheta) = \frac{1}{2}(h_{20}(\vartheta)z_1^2 + 2h_{11}(\vartheta)z_1z_2 + h_{02}(\vartheta)z_2^2). \tag{5.6}$$

There are no linear terms since the plane spanned by the eigenvectors s_1 and s_2 is tangent to the centre manifold at the origin. Third and higher order terms are dropped. The unknown coefficients $h_{20}, h_{11}, h_{02} \in \mathbb{X}_{\mathbb{R}^{2n}}$ can be determined by calculating the derivative of w and substituting that into the third equation of (5.5). The solution of the resulting linear boundary value problem, given in detail

in Orosz & Stépán (2004), is

$$\begin{bmatrix} h_{20}(\vartheta) \\ h_{11}(\vartheta) \\ h_{02}(\vartheta) \end{bmatrix} = \begin{bmatrix} H_1 \\ H_2 \\ -H_1 \end{bmatrix} \cos(2\omega\vartheta) + \begin{bmatrix} -H_2 \\ H_1 \\ H_2 \end{bmatrix} \sin(2\omega\vartheta) + \begin{bmatrix} H_0 \\ 0 \\ H_0 \end{bmatrix} - \begin{bmatrix} F_{20}^{(3-)} \\ 0 \\ F_{20}^{(3-)} \end{bmatrix} \vartheta, \quad (5.7)$$

where the vectors $H_0, H_1, H_2 \in \mathbb{R}^{2n}$ satisfy

$$\begin{bmatrix} \mathbf{L} + \mathbf{R} & 0 & 0 \\ 0 & \mathbf{L} + \mathbf{R}\cos(2\omega) & 2\omega\mathbf{I} + \mathbf{R}\sin(2\omega) \\ 0 & -(2\omega\mathbf{I} + \mathbf{R}\sin(2\omega)) & \mathbf{L} + \mathbf{R}\cos(2\omega) \end{bmatrix} \begin{bmatrix} H_0 \\ H_1 \\ H_2 \end{bmatrix} = -\frac{1}{2} \begin{bmatrix} F_{20}^{(3)} + F_{02}^{(3)} + 2F_{20}^{(3-)} \\ F_{20}^{(3)} - F_{02}^{(3)} \\ F_{11}^{(3)} \end{bmatrix}. \quad (5.8)$$

Here, we also used that

$$F_{jk}^{(3c)} = F_{jk}^{(3s)} = 0, \quad F_{20}^{(3-)} - F_{02}^{(3-)} = F_{11}^{(3-)} = 0, \quad \mathbf{R}F_{20}^{(3-)} = 0, \quad (5.9)$$

in accordance with equation (A 8).

One can find that the $2n$ -dimensional equation for H_0 is decoupled from the $4n$ -dimensional equation for H_1, H_2 in equation (5.8). Since $(\mathbf{L} + \mathbf{R})$ is singular due to the translational symmetry (4.5), the non-homogeneous equation for H_0 in (5.8) may seem not to be solvable. However, its right-hand side belongs to the image space of the coefficient matrix $(\mathbf{L} + \mathbf{R})$ due to the translational symmetry induced terms $F_{jk}^{(3-)}$. We obtain the solution

$$H_0 = \frac{b_{2cr}}{(b_{1cr})^2} \left(1 + \frac{\omega^2}{\alpha^2} \right) \begin{bmatrix} E \\ \kappa E \end{bmatrix}, \quad (5.10)$$

with the undetermined parameter κ that has no role in the following calculations.

At the same time, the non-homogeneous equation for H_1, H_2 in equation (5.8) is not effected by the vectors $F_{jk}^{(3-)}$. Using equation (3.17) and following the steps (A 10)–(A 14) of appendix A one can find the solution

$$\left. \begin{aligned} H_1 &= \frac{4b_{2cr}}{\omega^2 b_{1cr}} \left(\left(\eta - 4 \cot\left(\frac{k\pi}{n}\right) \right) \begin{bmatrix} 2\omega\tilde{C}, \\ \tilde{S} \end{bmatrix} + \mu \begin{bmatrix} 2\omega\tilde{S}, \\ -\tilde{C} \end{bmatrix} \right), \\ H_2 &= \frac{4b_{2cr}}{\omega^2 b_{1cr}} \left(\left(\eta - 4 \cot\left(\frac{k\pi}{n}\right) \right) \begin{bmatrix} 2\omega\tilde{S}, \\ -\tilde{C} \end{bmatrix} - \mu \begin{bmatrix} 2\omega\tilde{C}, \\ \tilde{S} \end{bmatrix} \right), \end{aligned} \right\} \quad (5.11)$$

where

$$\mu = -\frac{16b_{1cr} \omega^2}{\alpha \alpha^2 \left(1 + \frac{\omega^2}{\alpha^2}\right)^2}, \eta = \frac{8b_{1cr} \left(1 + 3\frac{\omega^2}{\alpha^2}\right)}{\omega \left(1 + \frac{\omega^2}{\alpha^2}\right)^2}, \tilde{C} = \begin{bmatrix} \cos\left(\frac{4k\pi}{n} 1\right) \\ \cos\left(\frac{4k\pi}{n} 2\right) \\ \vdots \\ \cos\left(\frac{4k\pi}{n} n\right) \end{bmatrix}, \tilde{S} = \begin{bmatrix} \sin\left(\frac{4k\pi}{n} 1\right) \\ \sin\left(\frac{4k\pi}{n} 2\right) \\ \vdots \\ \sin\left(\frac{4k\pi}{n} n\right) \end{bmatrix}. \tag{5.12}$$

Now, using equation (5.11) in (5.6) and (5.7), we can calculate $\mathbf{R}w(-1)$ which appears in the first two equations of (5.5). In this way, we obtain the flow restricted onto the two-dimensional centre manifold described by the ODEs

$$\begin{bmatrix} \dot{z}_1 \\ \dot{z}_2 \end{bmatrix} = \begin{bmatrix} 0 & \omega \\ -\omega & 0 \end{bmatrix} \begin{bmatrix} z_1 \\ z_2 \end{bmatrix} + \begin{bmatrix} \sum_{\substack{j+k=2,3 \\ j,k \geq 0}} f_{jk}^{(1)} z_1^j z_2^k \\ \sum_{\substack{j+k=2,3 \\ j,k \geq 0}} f_{jk}^{(2)} z_1^j z_2^k \end{bmatrix} + \begin{bmatrix} \sum_{\substack{j+k=3 \\ j,k \geq 0}} g_{jk}^{(1)} z_1^j z_2^k \\ \sum_{\substack{j+k=3 \\ j,k \geq 0}} g_{jk}^{(2)} z_1^j z_2^k \end{bmatrix}, \tag{5.13}$$

where the coefficients $f_{jk}^{(i)}$ have already been determined by equation (A 8) in (5.5), while the coefficients

$$\begin{aligned} g_{30}^{(1)} &= g_{12}^{(1)} = g_{21}^{(2)} = g_{03}^{(2)} \\ &= \frac{\mathcal{E} \frac{2\alpha(b_{2cr})^2}{(b_{1cr})^4} \cot\left(\frac{k\pi}{n}\right)}{\left(\eta - 4 \cot\left(\frac{k\pi}{n}\right)\right)^2 + \mu^2} \frac{\alpha}{\omega} \left(1 + \frac{\omega^2}{\alpha^2}\right) \left(\left(\eta - 4 \cot\left(\frac{k\pi}{n}\right)\right)\left(\omega + \frac{\omega}{\alpha} + \frac{\omega^3}{\alpha^2}\right)\right. \\ &\quad \left. + \mu \left(1 + 2\frac{\omega^2}{\alpha^2}\right)\right), \end{aligned} \tag{5.14}$$

originate in the terms involving $\mathbf{R}w(-1)$. To determine equation (5.14), the trigonometric identities (B 3)–(B 11) of appendix B have been used. The coefficients $g_{21}^{(1)} = g_{03}^{(1)} = -g_{30}^{(2)} = -g_{12}^{(2)}$ are not displayed, since they have no role in the following calculations.

We note that the coefficients $f_{jk}^{(i)}$ ($j + k = 2$) of the second-order terms are not changed by the centre-manifold reduction. The so-called Poincaré–Lyapunov constant in the Poincaré normal form of equation (5.13) can be determined by

the Bautin formula (Stépan 1989)

$$\begin{aligned} \Delta &= \frac{1}{8} \left(\frac{1}{\omega} ((f_{20}^{(1)} + f_{02}^{(1)})(-f_{11}^{(1)} + f_{20}^{(2)} - f_{02}^{(2)}) + (f_{20}^{(2)} + f_{02}^{(2)})(f_{20}^{(1)} - f_{02}^{(1)} + f_{11}^{(2)})) \right. \\ &\quad \left. + (3f_{30}^{(1)} + f_{12}^{(1)} + f_{21}^{(2)} + 3f_{03}^{(2)}) + (3g_{30}^{(1)} + g_{12}^{(1)} + g_{21}^{(2)} + 3g_{03}^{(2)}) \right) \\ &= \mathcal{E} \frac{\alpha}{4(b_{1\text{cr}})^3} \frac{\alpha}{\omega} \left(1 + \frac{\omega^2}{\alpha^2} \right) \left(\omega + \frac{\omega}{\alpha} + \frac{\omega^3}{\alpha^2} \right) \\ &\quad \times \frac{1}{2} \left(6b_{3\text{cr}} + \frac{(2b_{2\text{cr}})^2}{b_{1\text{cr}}} \frac{4 \cot\left(\frac{k\pi}{n}\right)}{(\eta - 4 \cot\left(\frac{k\pi}{n}\right))^2 + \mu^2} \left(\eta - 4 \cot\left(\frac{k\pi}{n}\right) + \mu \frac{1 + 2\frac{\omega^2}{\alpha^2}}{\omega + \frac{\omega}{\alpha} + \frac{\omega^3}{\alpha^2}} \right) \right). \end{aligned} \quad (5.15)$$

The bifurcation is supercritical for negative and subcritical for positive values of Δ . We found that $\Delta > 0$ is always true when $(k/n) \ll 1$ which is the case for real traffic situations (many vehicles n with a few waves k). This can be proven as is detailed below.

The first part of the expression (5.15) of Δ in front of the parenthesis is always positive, since $\mathcal{E}, b_{1\text{cr}}, \alpha, \omega > 0$. Within the parenthesis in equation (5.15), the first term is positive since equation (3.16) implies $b_{1\text{cr}} = \mathbf{V}'(h_{\text{cr}}^*) < 1/2$, which yields critical headway values h_{cr}^* such that $6b_{3\text{cr}} = \mathbf{V}'''(h_{\text{cr}}^*) > 0$; see figure 2*b,d*. The second term in the parenthesis in equation (5.15) contains the ratio of two complicated expressions, which by using equations (3.16) and (5.12), can be rearranged in the form

$$\begin{aligned} &4 \cot\left(\frac{k\pi}{n}\right) \left(\eta - 4 \cot\left(\frac{k\pi}{n}\right) + \mu \frac{1 + 2\frac{\omega^2}{\alpha^2}}{\omega + \frac{\omega}{\alpha} + \frac{\omega^3}{\alpha^2}} \right) \\ &= \left(4 \cot\left(\frac{k\pi}{n}\right) \right)^2 \left(\frac{\left(1 + \frac{\omega^2}{\alpha^2}\right) \left(\omega + \frac{\omega}{\alpha} + 3\frac{\omega^3}{\alpha^2}\right) - 4\frac{\omega^5}{\alpha^3}}{(\cos \omega - \frac{\omega}{\alpha} \sin \omega) \left(1 + \frac{\omega^2}{\alpha^2}\right) \left(\omega + \frac{\omega}{\alpha} + \frac{\omega^3}{\alpha^2}\right)} - 1 \right) \\ &:= \left(4 \cot\left(\frac{k\pi}{n}\right) \right)^2 \mathcal{N}(\omega, \alpha), \end{aligned} \quad (5.16)$$

and

$$\begin{aligned} &\left(\eta - 4 \cot\left(\frac{k\pi}{n}\right) \right)^2 + \mu^2 \\ &= \left(4 \cot\left(\frac{k\pi}{n}\right) \right)^2 \left(\frac{\left(1 + \frac{\omega^2}{\alpha^2}\right) \left(1 + 4\frac{\omega^2}{\alpha^2}\right) - 2(\cos \omega - \frac{\omega}{\alpha} \sin \omega) \left(1 + 3\frac{\omega^2}{\alpha^2}\right)}{(\cos \omega - \frac{\omega}{\alpha} \sin \omega)^2 \left(1 + \frac{\omega^2}{\alpha^2}\right)} + 1 \right) \\ &:= \left(4 \cot\left(\frac{k\pi}{n}\right) \right)^2 \mathcal{D}(\omega, \alpha) > 0. \end{aligned} \quad (5.17)$$

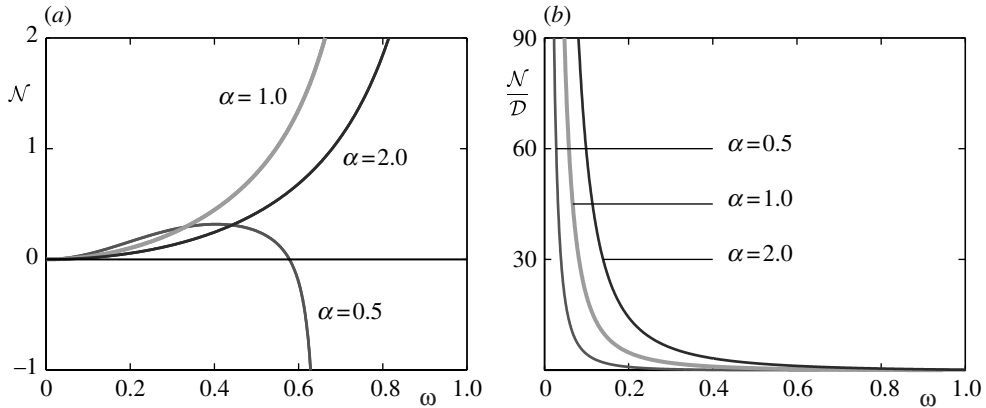


Figure 3. Quantities defined by (5.16) and (5.17) as a function of the frequency ω , for representative values of parameter α . (a) Numerator $\mathcal{N}(\omega, \alpha)$ and (b) ratio $\mathcal{N}(\omega, \alpha)/\mathcal{D}(\omega, \alpha)$.

Since equation (5.17) is always positive, the sign of equation (5.16) is crucial for deciding the overall sign of Δ . According to equation (3.16) $\omega \in (0, k\pi/n)$, that is, the realistic case $(k/n) \ll 1$ implies the oscillation frequency $\omega \ll 1$.

Figure 3a shows the numerator $\mathcal{N}(\omega, \alpha)$ for some particular values of α demonstrating that $\mathcal{N}(\omega, \alpha) > 0$ for $\omega \ll 1$. Note that if $\alpha \rightarrow 0$ then $\mathcal{N}(\omega, \alpha)$ may become negative (see figure 3a for $\alpha = 0.5$), but this is a physically unrealistic case where drivers intend to reach their desired speed v^0 extremely slowly.

Moreover, the ratio of equations (5.16) and (5.17), $\mathcal{N}(\omega, \alpha)/\mathcal{D}(\omega, \alpha)$, is not only positive for $\omega \ll 1$ but also $\mathcal{N}(\omega, \alpha)/\mathcal{D}(\omega, \alpha) \rightarrow \infty$ when $\omega \rightarrow 0$ (i.e. when $n \rightarrow \infty$) as shown in figure 3b. This feature provides robustness for subcriticality. Note that subcriticality also occurs for optimal velocity functions different from equation (2.2), e.g. for those that are considered in Orosz *et al.* (2004).

Using definition (3.6), formulae (3.18) and (3.22) and expressions (5.15)–(5.17), the amplitude A of the unstable oscillations is obtained in the form

$$A = \sqrt{-\frac{\text{Re}(\lambda'_1(h_{\text{cr}}^*))}{\Delta} (h^* - h_{\text{cr}}^*)} = \frac{\omega}{\sin(\frac{k\pi}{n})} \sqrt{-2 \frac{\mathbf{V}''(h_{\text{cr}}^*)(h^* - h_{\text{cr}}^*)}{\mathbf{V}'''(h_{\text{cr}}^*) + \frac{(\mathbf{V}''(h_{\text{cr}}^*))^2}{\mathbf{V}'(h_{\text{cr}}^*)} \frac{\mathcal{N}(\omega, \alpha)}{\mathcal{D}(\omega, \alpha)}}}. \tag{5.18}$$

Thus, the first Fourier term of the oscillation restricted onto the centre manifold is

$$\begin{bmatrix} z_1(t) \\ z_2(t) \end{bmatrix} = A \begin{bmatrix} \cos(\omega t) \\ -\sin(\omega t) \end{bmatrix}. \tag{5.19}$$

Since close to the critical bifurcation parameter h_{cr}^* , we have $y_t(\vartheta) \approx z_1(t)s_1(\vartheta) + z_2(t)s_2(\vartheta)$, equation (5.19) yields

$$\begin{aligned} y(t) = y_t(0) &\approx z_1(t)s_1(0) + z_2(t)s_2(0) = A(s_1(0)\cos(\omega t) - s_2(0)\sin(\omega t)) \\ &= A(S_1\cos(\omega t) - S_2\sin(\omega t)), \end{aligned} \tag{5.20}$$

where the vectors S_1, S_2 are given in equation (4.29).

The parameter $v^0 > 0$ enters Δ and A via the derivatives $\mathbf{V}'(h_{\text{cr}}^*) = b_{1\text{cr}}$, $\mathbf{V}''(h_{\text{cr}}^*) = 2b_{2\text{cr}}$ and $\mathbf{V}'''(h_{\text{cr}}^*) = 6b_{3\text{cr}}$ which are all proportional to v^0 . Consequently, Δ depends linearly on v^0 causing no sign change and v^0 disappears from A . Furthermore, v^0 is embedded in the critical parameter h_{cr}^* which is determined from equation (3.16) by inverting $\mathbf{V}'(h_{\text{cr}}^*) = b_{1\text{cr}}$. However, one may check that this is relevant for $k/n \simeq 1/2$ only, when small v^0 may result in supercriticality as demonstrated in Orosz *et al.* (2004). In contrast, the realistic case $k/n \ll 1$ leads to robust subcriticality as explained in §6 and also demonstrated in Orosz *et al.* (2005).

Note that zero reaction time delay results in $\mathcal{N}(\omega, \alpha)/\mathcal{D}(\omega, \alpha) \equiv -1$ as shown in Gasser *et al.* (2004). In that case, subcriticality appears only for extremely high values of the desired speed v^0 when the term $6b_{3\text{cr}}$ becomes greater than $(2b_{2\text{cr}})^2/b_{1\text{cr}}$ at the critical points (of the non-delayed model). Consequently, the presence of the drivers' reaction-time delay has an essential role in the robustness of the subcritical nature of the Hopf bifurcation. This subcriticality explains how traffic waves can be formed when the uniform flow equilibrium is stable, as is detailed in the subsequent section.

6. Physical interpretation of results

The unstable periodic motion given in equation (5.20) corresponds to a spatial wave formation in the traffic flow, which is actually unstable. Substituting (4.29) into (5.20) and using definition (3.7), one can determine the velocity perturbation as

$$\dot{x}_i^{\text{p}}(t) = A \cos\left(\frac{2\pi k}{n}i + \omega t\right), \quad i = 1, \dots, n. \quad (6.1)$$

The interpretation of this perturbation mode is a wave travelling opposite to the car flow with spatial wave number k (i.e. with spatial wavelength $L/k = h^*n/k$). The related wave speed is

$$c_{\text{wave}}^{\text{p}} = -\frac{n}{2k\pi} h^* \omega < 0, \quad (6.2)$$

where the elimination of the frequency ω with the help of equation (3.18) leads to

$$c_{\text{wave}}^{\text{p}} = -h^* b_{1\text{cr}} \left(1 - \mathcal{O}\left(\frac{k\pi}{n}\right)^2\right). \quad (6.3)$$

Since the uniform flow equilibrium (3.1) travels with speed $v^* = \mathbf{V}(h^*)$, the speed of the arising wave is

$$c_{\text{wave}} = v^* + c_{\text{wave}}^{\text{p}} = \mathbf{V}(h^*) - h^* \mathbf{V}'(h_{\text{cr}}^*) \left(1 - \mathcal{O}\left(\frac{k\pi}{n}\right)^2\right). \quad (6.4)$$

By considering the optimal velocity function (2.2), we obtain $c_{\text{wave}} < 0$, that is, the resulting wave propagates in the opposite direction to the flow of vehicles. Note that the non-delayed model introduced in Bando *et al.* (1995) exhibits the same wave speed apart from some differences in the coefficient of the correction term $\mathcal{O}(k\pi/n)^2$. If one neglects this correction term, the wave speed becomes

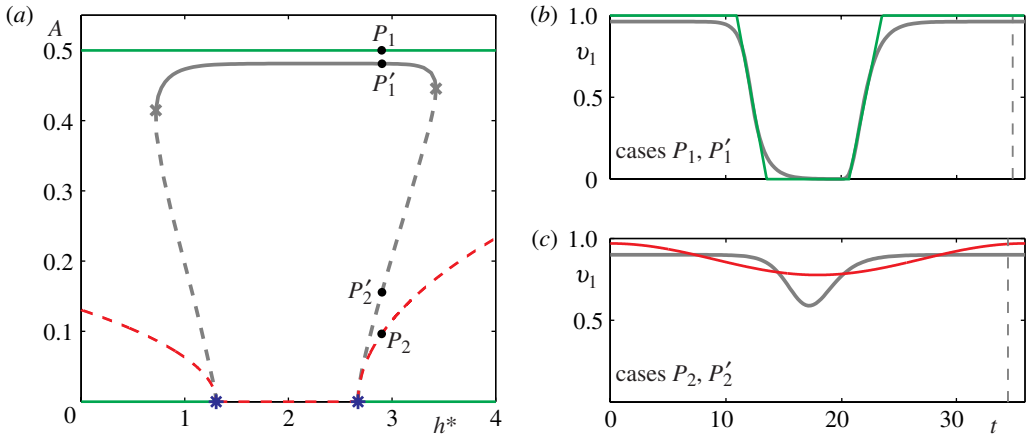


Figure 4. The amplitude A of velocity oscillations as a function of the average headway parameter h^* (a) and the corresponding velocity profiles at $h^* = 2.9$ (b) and (c) for $n = 9$ cars, $k = 1$ wave and parameters $\alpha = 1.0$, $v^0 = 1.0$. (a) Horizontal axis ($A \equiv 0$) represents the uniform flow equilibrium and the analytical results are coloured: green solid and red dashed curves represent stable and unstable branches, respectively, and blue stars stand for Hopf bifurcations. Grey curves correspond to numerical continuation results: solid and dashed curves refer to stable and unstable states and grey crosses represent fold bifurcations. The points marked by P_1, P'_1 and P_2, P'_2 refer to the velocity profiles shown in panels (b) and (c), respectively. (b) Stable stop-and-go oscillations are shown for point P_1 in green and for point P'_1 in grey and (c) unstable oscillations are displayed for point P_2 in red and for point P'_2 in grey.

independent of n and k , which corresponds to the results obtained from continuum models; see e.g. Whitham (1999).

In order to check the reliability of the Poincaré–Lyapunov constant (5.15) and the amplitude estimation (5.18), we compare these analytical results with those obtained by numerical continuation techniques with the package DDE-BIFTOOL (Engelborghs *et al.* 2001). In figure 4a, we demonstrate the subcriticality for $n = 9$ cars and $k = 1$ wave. The horizontal axis corresponds to the uniform flow equilibrium, that is, stable for small and large values of h^* (shown by green solid line) but unstable for intermediate values of h^* (shown by red dashed line) in accordance with formula (3.16) and figure 2b. The Hopf bifurcations, where the equilibrium loses its stability, are marked by blue stars. The branches of the arising unstable periodic motions given by equation (5.18) are shown as red dashed curves.

In §2, conditions (i)–(iii) require that the optimal velocity function is bounded so that $\mathbf{V} \in [0, v^0]$; see figure 2a. Maximum principles show that for $t \rightarrow \infty$ the velocity of *any* solution is contained by the interval $[0, v^0]$. This suggests that ‘outside’ the unstable oscillating state there exists an attractive oscillating state which may include stopping, accelerating, travelling with the desired speed v^0 , and decelerating. The amplitude of this solution is defined as $A = (\max \dot{x}_i(t) - \min \dot{x}_i(t))/2 \simeq (v^0 - 0)/2 = v^0/2$. In figure 4a the horizontal green line at $A = v^0/2$ represents this stable *stop-and-go oscillation*. The corresponding *stop-and-go wave* propagates against the traffic flow, since vehicles leave the traffic jam at the front and enter it at the rear; see figure 1. The above heuristic construction reveals the existence of bistability on each side of

the unstable equilibrium between the Hopf bifurcation point and the point where the branches of unstable and stable oscillations intersect each other (outside the frame in figure 4a). For such parameters, depending on the initial condition, the system either tends to the uniform flow equilibrium or to the stop-and-go wave.

In figure 4a, we also displayed the results of numerical continuation carried out with the package DDE-BIFTOOL (Engelborghs *et al.* 2001). Grey solid curves represent stable oscillations while grey dashed curves represent unstable ones. The fold bifurcation points, where the branches of stable and unstable oscillations meet, are marked by grey crosses. The comparison of the results shows that the analytical approximation of the unstable oscillations is quantitatively reliable in the vicinity of the Hopf bifurcation points. The heuristic amplitude $v^0/2$ of the stop-and-go oscillations is slightly larger than the numerically computed ones. The analytically suggested bistable region is larger than the computed one (between the Hopf point and the fold point), since the third degree approximation is not able to predict fold bifurcations of periodic solutions. In order to find these fold bifurcation points, it is necessary to use numerical continuation techniques as presented in Orosz *et al.* (2005). Nevertheless, qualitatively the same structure is obtained by the two different techniques.

As was already mentioned in §3, the wave numbers $k > 1$ are related to Hopf bifurcations in the parameter region, where the uniform flow equilibrium is already unstable. This also means that the corresponding oscillations for $k > 1$ are unstable independently of the criticality of these Hopf bifurcations. Still, we found that these Hopf bifurcations are all robustly subcritical for any wave number k (except for large $k/n \simeq 1/2$). Consequently, the only stable oscillating state is the stop-and-go motion for $k=1$. On the other hand, several unstable solutions may coexist as is explained in Orosz *et al.* (2005). Note that analytical and numerical results agree better as the wave number k is increased because the oscillating solution becomes more harmonic.

To represent the features of vehicles' motions, the velocity oscillation profiles of the first vehicle are shown in figure 4b,c for the points P_1, P'_1 and P_2, P'_2 marked in figure 4a, for headway $h^* = 2.9$. Again, the coloured curves correspond to the analytical results, while the grey curves are obtained by numerical continuation. In figure 4b,c, the time window of each panel is chosen to be the period of the first Fourier approximation given by equation (3.18) (red curve in figure 4c) and the dashed vertical lines indicate oscillation periods computed numerically with DDE-BIFTOOL.

Figure 4b shows the stop-and-go oscillations. The heuristic construction (green curve) is obtained by assuming that the stopping and flowing states are connected with states of constant acceleration/deceleration, which is qualitatively a good approximation of the numerical result (grey curve). Figure 4c compares the unstable periodic motions computed analytically (red curve) from the Hopf calculation with those from numerical continuation (grey curve).

For a perturbation 'smaller' than the unstable oscillation, the system approaches the uniform flow equilibrium. If a larger perturbation is applied then the system develops stop-and-go oscillations and a spatial stop-and-go travelling wave appears as demonstrated in figure 1. Since the period of the stable and unstable oscillations are close to each other, the stable stop-and-go wave travels approximately with the speed of the unstable travelling wave; see equation (6.4) for $k=1$.

7. Conclusion

A nonlinear car-following model has been investigated with special attention paid to the reaction-time delay of drivers. By considering the average headway as a bifurcation parameter, Hopf bifurcations were identified. In order to investigate the resulting periodic motions, the singularities related to the essential translational symmetry had to be eliminated. Then the Hopf bifurcations were found to be robustly subcritical leading to bistability between the uniform flow equilibrium and a stop-and-go wave. The appearing oscillations manifest themselves as spatial waves propagating backward along the circular road.

In the non-delayed model of Bando *et al.* (1995), subcriticality and bistability occur only for extremely high values of the desired speed v^0 , as it is demonstrated in Gasser *et al.* (2004). We proved that subcriticality and bistability are robust features of the system due to the drivers' reaction-time delay, even for moderate values of the desired speed. This delay, which is smaller than the macroscopic time-scales of traffic flow, plays an essential role in this complex system because it changes the qualitative nonlinear dynamics of traffic.

Due to the subcriticality, stop-and-go traffic jams can develop for large enough perturbations even when the desired uniform flow is linearly stable. These perturbations can be caused, for example, by a slower vehicle (such as a lorry) joining the inner lane flow for a short-time interval via changing lanes. It is essential to limit these unwanted events, for example, by introducing temporary regulations provided by overhead gantries. Still, if a backward travelling wave shows up without stoppings, it either dies out by itself or gets worse ending up as a persistent stop-and-go travelling wave. In order to dissolve this undesired situation, an appropriate control can be applied using temporary speed limits given by overhead gantries that can lead the traffic back 'inside' the unstable travelling wave and then to reach the desired uniform flow. For example, the MIDAS system (Lunt & Wilson 2003) installed on the M25 motorway around London is able to provide the necessary instructions for drivers.

The authors acknowledge with thanks discussions with and comments of Eddie Wilson and Bernd Krauskopf on traffic dynamics and on numerical bifurcation analysis. This research was supported by the University of Bristol under a Postgraduate Research Scholarship and by the Hungarian National Science Foundation under grant no. OTKA T043368.

Appendix A. Solutions of algebraic equations

Using formula (3.17) for the Hopf boundary, the $4n$ -dimensional equation (4.26) leads to

$$\left. \begin{aligned} S_{2,i} &= \omega S_{1,n+i} \\ S_{2,n+i} &= -\frac{1}{\omega} S_{1,i} \end{aligned} \right\} \text{ for } i = 1, \dots, n, \quad (\text{A } 1)$$

and to the $2n$ -dimensional equation

$$\begin{bmatrix} -\frac{1}{\omega} \cot\left(\frac{k\pi}{n}\right)A & B \\ B & \frac{1}{\omega} \cot\left(\frac{k\pi}{n}\right)A \end{bmatrix} S_1 = 0, \quad (\text{A } 2)$$

where $A \in \mathbb{R}^{n \times n}$ is defined by equation (3.10) and $B \in \mathbb{R}^{n \times n}$ is given by

$$B = \begin{bmatrix} \ddots & \ddots & & & \\ & 1 & 1 & & \\ & & \ddots & \ddots & \\ 1 & & & & \ddots \end{bmatrix}. \quad (\text{A } 3)$$

Solving (A 2) one may obtain the solution (4.27) for S_1 and S_2 .

The application of (3.17) simplifies the $4n$ -dimensional equation (4.32) to

$$\left. \begin{aligned} N_{1,n+i} &= \alpha N_{1,i} + \omega N_{2,i} \\ N_{2,n+i} &= -\omega N_{1,i} + \alpha N_{2,i} \end{aligned} \right\} \text{ for } i = 1, \dots, n, \quad (\text{A } 4)$$

and to the $2n$ -dimensional equation

$$\begin{bmatrix} -\cot\left(\frac{k\pi}{n}\right)A & B \\ B & \cot\left(\frac{k\pi}{n}\right)A \end{bmatrix} N_U = 0, \quad (\text{A } 5)$$

where $A, B \in \mathbb{R}^{n \times n}$ are given by (3.10) and (A 3) and $N_U \in \mathbb{R}^{2n}$ is defined as

$$\left. \begin{aligned} N_{U,i} &= N_{1,i} \\ N_{U,n+i} &= N_{2,i} \end{aligned} \right\} \text{ for } i = 1, \dots, n. \quad (\text{A } 6)$$

The solution of (A 5) can be written as

$$N_U = \hat{u} \begin{bmatrix} C \\ S \end{bmatrix} + \hat{v} \begin{bmatrix} S \\ -C \end{bmatrix}, \quad (\text{A } 7)$$

where the vectors $C, S \in \mathbb{R}^n$ are defined by equation (4.28). This leads to the solution (4.33) for N_1 and N_2 .

The coefficients in (5.5) are as follows:

$$\begin{aligned}
 f_{jk}^{(1)} &= f_{jk}^{(2)} = 0, \text{ for } j + k = 2, \\
 f_{30}^{(1)} &= f_{12}^{(1)} = f_{21}^{(2)} = f_{03}^{(2)} = \varepsilon \frac{3\alpha b_{3cr}}{4(b_{1cr})^3} \frac{\alpha}{\omega} \left(1 + \frac{\omega^2}{\alpha^2}\right) \left(\omega + \frac{\omega}{\alpha} + \frac{\omega^3}{\alpha^2}\right), \\
 f_{21}^{(1)} &= f_{03}^{(1)} = -f_{30}^{(2)} = -f_{12}^{(2)} = \varepsilon \frac{3\alpha b_{3cr}}{4(b_{1cr})^3} \frac{\alpha}{\omega} \left(1 + \frac{\omega^2}{\alpha^2}\right) \left(1 + 2\frac{\omega^2}{\alpha^2}\right), \\
 F_{10}^{(1)} &= \varepsilon \frac{2b_{2cr}}{n(b_{1cr})^2} \begin{bmatrix} \left(3 + \alpha - \frac{\omega^2}{\alpha}\right) \tilde{C} + \left(\frac{\alpha}{\omega} - 2\omega - 2\frac{\omega}{\alpha}\right) \tilde{S} + \left(1 + \alpha + \frac{\omega^2}{\alpha}\right) E \\ 0 \end{bmatrix}, \\
 F_{01}^{(1)} &= \varepsilon \frac{2b_{2cr}}{n(b_{1cr})^2} \begin{bmatrix} -\left(\frac{\alpha}{\omega} - 2\omega - 2\frac{\omega}{\alpha}\right) \tilde{C} + \left(3 + \alpha - \frac{\omega^2}{\alpha}\right) \tilde{S} + \left(\frac{\alpha}{\omega} + 2\frac{\omega}{\alpha}\right) E \\ 0 \end{bmatrix}, \\
 F_{10}^{(2)} &= \varepsilon \frac{2b_{2cr}}{n(b_{1cr})^2} \begin{bmatrix} -\left(\frac{\alpha}{\omega} - 2\omega - 2\frac{\omega}{\alpha}\right) \tilde{C} + \left(3 + \alpha - \frac{\omega^2}{\alpha}\right) \tilde{S} - \left(\frac{\alpha}{\omega} + 2\frac{\omega}{\alpha}\right) E \\ 0 \end{bmatrix}, \\
 F_{01}^{(2)} &= \varepsilon \frac{2b_{2cr}}{n(b_{1cr})^2} \begin{bmatrix} -\left(3 + \alpha - \frac{\omega^2}{\alpha}\right) \tilde{C} - \left(\frac{\alpha}{\omega} - 2\omega - 2\frac{\omega}{\alpha}\right) \tilde{S} + \left(1 + \alpha + \frac{\omega^2}{\alpha}\right) E \\ 0 \end{bmatrix}, \\
 F_{jk}^{(3c)} &= F_{jk}^{(3s)} = 0, \\
 F_{20}^{(3-)} &= F_{02}^{(3-)} = -\frac{b_{2cr}}{(b_{1cr})^2} \left(1 + \frac{\omega^2}{\alpha^2}\right) \begin{bmatrix} 0 \\ E \end{bmatrix}, \\
 F_{11}^{(3-)} &= 0, \\
 F_{20}^{(3)} &= \frac{b_{2cr}}{(b_{1cr})^2} \begin{bmatrix} \left(1 - \frac{\omega^2}{\alpha^2}\right) \tilde{C} - 2\frac{\omega}{\alpha} \tilde{S} + \left(1 + \frac{\omega^2}{\alpha^2}\right) E \\ 0 \end{bmatrix}, \\
 F_{11}^{(3)} &= \frac{2b_{2cr}}{(b_{1cr})^2} \begin{bmatrix} 2\frac{\omega}{\alpha} \tilde{C} + \left(1 - \frac{\omega^2}{\alpha^2}\right) \tilde{S} \\ 0 \end{bmatrix}, \\
 F_{02}^{(3)} &= \frac{b_{2cr}}{(b_{1cr})^2} \begin{bmatrix} -\left(1 - \frac{\omega^2}{\alpha^2}\right) \tilde{C} + 2\frac{\omega}{\alpha} \tilde{S} + \left(1 + \frac{\omega^2}{\alpha^2}\right) E \\ 0 \end{bmatrix},
 \end{aligned}
 \tag{A8}$$

where \mathcal{E} is given by equation (3.21), each component of $E \in \mathbb{R}^n$ is 1, and the vectors $\tilde{C}, \tilde{S} \in \mathbb{R}^n$ are defined by

$$\tilde{C} = \begin{bmatrix} \cos\left(\frac{4k\pi}{n}1\right) \\ \cos\left(\frac{4k\pi}{n}2\right) \\ \vdots \\ \cos\left(\frac{4k\pi}{n}n\right) \end{bmatrix}, \quad \tilde{S} = \begin{bmatrix} \sin\left(\frac{4k\pi}{n}1\right) \\ \sin\left(\frac{4k\pi}{n}2\right) \\ \vdots \\ \sin\left(\frac{4k\pi}{n}n\right) \end{bmatrix}. \quad (\text{A } 9)$$

Using (3.17), the $4n$ -dimensional equation for H_1, H_2 in (5.8) leads to

$$\left. \begin{aligned} H_{1,i} &= -2\omega H_{2,n+i} \\ H_{2,i} &= 2\omega H_{1,n+i} \end{aligned} \right\} \text{ for } i = 1, \dots, n, \quad (\text{A } 10)$$

and to the $2n$ -dimensional equation

$$\begin{aligned} & \begin{bmatrix} \mu \sin^2\left(\frac{k\pi}{n}\right) \text{I} - \cos\left(\frac{2k\pi}{n}\right) A & \eta \sin^2\left(\frac{k\pi}{n}\right) \text{I} - \sin\left(\frac{2k\pi}{n}\right) A \\ -\left(\eta \sin^2\left(\frac{k\pi}{n}\right) \text{I} - \sin\left(\frac{2k\pi}{n}\right) A\right) & \mu \sin^2\left(\frac{k\pi}{n}\right) \text{I} - \cos\left(\frac{2k\pi}{n}\right) A \end{bmatrix} H_{\cup} \\ &= -\frac{4b_{2\text{cr}}}{\omega^2 b_{1\text{cr}}} \sin^2\left(\frac{k\pi}{n}\right) \begin{bmatrix} \tilde{C} \\ \tilde{S} \end{bmatrix}, \end{aligned} \quad (\text{A } 11)$$

where $\text{I} \in \mathbb{R}^{n \times n}$ is the identity matrix, $A \in \mathbb{R}^{n \times n}$ and $\tilde{C}, \tilde{S} \in \mathbb{R}^n$ are given by (3.10) and (A 9), the vector $H_{\cup} \in \mathbb{R}^{2n}$ is defined as

$$\left. \begin{aligned} H_{\cup,i} &= H_{1,n+i} \\ H_{\cup,n+i} &= H_{2,n+i} \end{aligned} \right\} \text{ for } i = 1, \dots, n, \quad (\text{A } 12)$$

and the new parameters are

$$\mu = -\frac{16b_{1\text{cr}} \omega^2}{\alpha \alpha^2 \left(1 + \frac{\omega^2}{\alpha^2}\right)^2}, \quad \eta = \frac{8b_{1\text{cr}} \left(1 + 3\frac{\omega^2}{\alpha^2}\right)}{\omega \left(1 + \frac{\omega^2}{\alpha^2}\right)^2}. \quad (\text{A } 13)$$

The solution of (A 11) is given by

$$H_U = \frac{-\frac{4b_{2cr}}{\omega^2 b_{1cr}}}{\left(\eta - 4 \cot\left(\frac{k\pi}{n}\right)\right)^2 + \mu^2} \left(\mu \begin{bmatrix} \tilde{C} \\ \tilde{S} \end{bmatrix} + \left(\eta - 4 \cot\left(\frac{k\pi}{n}\right)\right) \begin{bmatrix} -\tilde{S} \\ \tilde{C} \end{bmatrix} \right), \tag{A 14}$$

which leads to the solution (5.11) for H_1 and H_2 .

Appendix B. Trigonometric identities

Considering the wave numbers $k = 1, \dots, n/2$ (even n) or $k = 1, \dots, (n-1)/2$ (odd n)

$$\sum_{i=1}^n \exp\left(i\rho \frac{2k\pi}{n} i\right) = \begin{cases} 0, & \text{if } k \neq n/\rho, \\ n, & \text{if } k = n/\rho, \end{cases} \tag{B 1}$$

can be written where $i^2 = -1$ and $\rho = 1, \dots, 4$. Therefore, the following identities can be proven. In first order,

$$\sum_{i=1}^n \cos\left(\frac{2k\pi}{n} i\right) = \sum_{i=1}^n \sin\left(\frac{2k\pi}{n} i\right) = 0. \tag{B 2}$$

In second order,

$$\sum_{i=1}^n \cos^2\left(\frac{2k\pi}{n} i\right) = \begin{cases} n/2, & \text{if } k \neq n/2, \\ n, & \text{if } k = n/2, \end{cases} \tag{B 3}$$

$$\sum_{i=1}^n \sin^2\left(\frac{2k\pi}{n} i\right) = \begin{cases} n/2, & \text{if } k \neq n/2, \\ 0, & \text{if } k = n/2, \end{cases} \tag{B 4}$$

$$\sum_{i=1}^n \cos\left(\frac{2k\pi}{n} i\right) \sin\left(\frac{2k\pi}{n} i\right) = 0. \tag{B 5}$$

In third order,

$$\sum_{i=1}^n \cos^3\left(\frac{2k\pi}{n} i\right) = -\sum_{i=1}^n \cos\left(\frac{2k\pi}{n} i\right) \sin^2\left(\frac{2k\pi}{n} i\right) = \begin{cases} 0, & \text{if } k \neq n/3, \\ n/4, & \text{if } k = n/3, \end{cases} \tag{B 6}$$

$$\sum_{i=1}^n \sin^3\left(\frac{2k\pi}{n} i\right) = \sum_{i=1}^n \cos^2\left(\frac{2k\pi}{n} i\right) \sin\left(\frac{2k\pi}{n} i\right) = 0. \tag{B 7}$$

In fourth order,

$$\sum_{i=1}^n \cos^4\left(\frac{2k\pi}{n}i\right) = \begin{cases} 3n/8, & \text{if } k \neq n/2 \text{ and } k \neq n/4, \\ n, & \text{if } k = n/2, \\ n/2, & \text{if } k = n/4, \end{cases} \quad (\text{B } 8)$$

$$\sum_{i=1}^n \sin^4\left(\frac{2k\pi}{n}i\right) = \begin{cases} 3n/8, & \text{if } k \neq n/2 \text{ and } k \neq n/4, \\ 0, & \text{if } k = n/2, \\ n/2, & \text{if } k = n/4, \end{cases} \quad (\text{B } 9)$$

$$\sum_{i=1}^n \cos^2\left(\frac{2k\pi}{n}i\right) \sin^2\left(\frac{2k\pi}{n}i\right) = \begin{cases} n/8, & \text{if } k \neq n/2 \text{ and } k \neq n/4, \\ 0, & \text{if } k = n/2, \\ 0, & \text{if } k = n/4, \end{cases} \quad (\text{B } 10)$$

$$\sum_{i=1}^n \cos^3\left(\frac{2k\pi}{n}i\right) \sin\left(\frac{2k\pi}{n}i\right) = \sum_{i=1}^n \cos\left(\frac{2k\pi}{n}i\right) \sin^3\left(\frac{2k\pi}{n}i\right) = 0. \quad (\text{B } 11)$$

References

- Bando, M., Hasebe, K., Nakayama, A., Shibata, A. & Sugiyama, Y. 1995 Dynamical model of traffic congestion and numerical simulation. *Phys. Rev. E* **51**, 1035–1042. (doi:10.1103/PhysRevE.51.1035)
- Bando, M., Hasebe, K., Nakanishi, K. & Nakayama, A. 1998 Analysis of optimal velocity model with explicit delay. *Phys. Rev. E* **58**, 5429–5435. (doi:10.1103/PhysRevE.58.5429)
- Berg, P. & Wilson, R. E. 2005 Bifurcation analysis of meta-stability and waves of the OV model. In *Traffic and granular flow '03* (ed. S. P. Hoogendoorn, S. Luding, P. H. L. Bovy, M. Schreckenberg & D. E. Wolf). Berlin: Springer.
- Campbell, S. A. & Bélair, J. 1995 Analytical and symbolically-assisted investigations of Hopf bifurcations in delay-differential equations. *Can. Appl. Math. Q.* **3**, 137–154.
- Davis, L. C. 2003 Modification of the optimal velocity traffic model to include delay due to driver reaction time. *Physica A* **319**, 557–567. (doi:10.1016/S0378-4371(02)01457-7)
- Diekmann, O., van Gils, S. A., Verduyn Lunel, S. M. & Walther, H. O. 1995 *Delay equations: functional-, complex-, and nonlinear analysis*. Applied mathematical sciences, vol. 110. New York: Springer.
- Doedel E. J., Champneys A. R., Fairgrieve T. F., Kuznetsov Yu. A., Sandstede B. & Wang X. 1997 Auto97: continuation and bifurcation software for ordinary differential equations. Technical report, Department of Computer Science, Concordia University. <http://indy.cs.concordia.ca/auto/>.
- Engelborghs K., Luzyanina T. & Samaey G. 2001 Dde-Biftool v. 2.00: a Matlab package for bifurcation analysis of delay differential equations. Technical Report TW-330, Department of Computer Science, Katholieke Universiteit Leuven, Belgium. <http://www.cs.kuleuven.ac.be/koen/delay/ddebiftool.shtml>.
- Gasser, I., Siritto, G. & Werner, B. 2004 Bifurcation analysis of a class of ‘car-following’ traffic models. *Physica D* **197**, 222–241. (doi:10.1016/j.physd.2004.07.008)
- Guckenheimer, J. & Holmes, P. 1997 *Nonlinear oscillations, dynamical systems, and bifurcations of vector fields*. Applied mathematical sciences, vol. 42, 3rd edn. New York: Springer.
- Hale, J. K. & Verduyn Lunel, S. M. 1993 *Introduction to functional differential equations*. Applied mathematical sciences, vol. 99. New York: Springer.

- Hale, J. K., Magalhães, L. T. & Oliva, W. M. 2002 *Dynamics in infinite dimensions*. Applied mathematical sciences, vol. 47, 2nd edn. New York: Springer.
- Hassard, B. D., Kazarinoff, N. D. & Wan, Y.-H. 1981 *Theory and applications of Hopf bifurcation*. London Mathematical Society Lecture Note Series, vol. 41. Cambridge: Cambridge University Press.
- Kerner, B. S. 1999 The physics of traffic. *Phys. World* **8**, 25–30.
- Kolmanovskii, V. B. & Myshkis, A. D. 1999 *Introduction to the theory and applications of functional differential equations*. Mathematics and its applications, vol. 463. London: Kluwer Academic Publishers.
- Kuznetsov, Yu. A. 1998 *Elements of applied bifurcation theory*. Applied mathematical sciences, vol. 112, 2nd edn. New York: Springer.
- Lunt G. & Wilson R. E. 2003. New data sets and improved models of highway traffic. In *Proc. 35th UTSG Conf.* University of Loughborough, England.
- Orosz, G. 2004 Hopf bifurcation calculations in delayed systems. *Periodica Polytechnica* **48**, 189–200.
- Orosz, G. & Stépán, G. 2004 Hopf bifurcation calculations in delayed systems with translational symmetry. *J. Nonlin. Sci.* **14**, 505–528. (doi:10.1007/s00332-004-0625-4)
- Orosz, G., Wilson, R. E. & Krauskopf, B. 2004 Global bifurcation investigation of an optimal velocity traffic model with driver reaction time. *Phys. Rev. E* **70**, 026 207. (doi:10.1103/PhysRevE.70.026207)
- Orosz, G., Krauskopf, B. & Wilson, R. E. 2005 Bifurcations and multiple traffic jams in a car-following model with reaction-time delay. *Physica D* **211**, 277–293. (doi:10.1016/j.physd.2005.09.004)
- Rottschäfer, V. & Krauskopf, B. 2004 A three-parameter study of external cavity modes in semiconductor lasers with optical feedback. In *Fifth IFAC workshop on time-delay systems* (ed. W. Michiels & D. Roose). Leuven, Belgium: International Federation of Automatic Control (IFAC).
- Stépán, G. 1986 Great delay in a predator-prey model. *Nonlin. Anal. TMA* **10**, 913–929. (doi:10.1016/0362-546X(86)90078-7)
- Stépán, G. 1989 *Retarded dynamical systems: stability and characteristic functions*. Pitman research notes in mathematics, vol. 210. Essex, England: Longman.
- Stone, E. & Campbell, S. A. 2004 Stability and bifurcation analysis of a nonlinear DDE model for drilling. *J. Nonlin. Sci.* **14**, 27–57. (doi:10.1007/s00332-003-0553-1)
- Verduyn Lunel, S. M. & Krauskopf, B. 2000 The mathematics of delay equations with an application to the Lang-Kobayashi equations. In *Fundamental issues of nonlinear laser dynamics* (ed. B. Krauskopf & D. Lenstra), vol. 548, pp. 66–86. Melville, New York: American Institute of Physics.
- Whitham, G. B. 1999 *Linear and nonlinear waves*. New York: Wiley.